Forest Science, Vol 40, No 4, pp 601–617

Simulations of Buoyancy-Generated Horizontal Roll Vortices over Multiple Heating Lines

W.E. HEILMAN

ABSTRACT. A two-dimensional nonhydrostatic atmospheric model is used to simulate the boundary-layer circulations that develop from multiple lines of extremely high surface temperatures. Numerical simulations are carried out to investigate the role of buoyancy and ambient crossflow effects in generating horizontal roll vortices in the vicinity of adjacent wildland fire perimeters. Numerical results suggest that the downdraft segments of buoyancy-generated horizontal roll vortices can be reinforced when multiple heating lines are present, with the degree of reinforcement dependent on the heating-line spacing. Significant low-level horizontal flow directly over the bounding heating lines is observed in some simulations, suggesting a mechanism for low-level flame migration in actual wildland fires. Multiple heating lines also affect the development and behavior of buoyancy-generated horizontal roll vortices when ambient crossflows are present. Simulations indicate that vortices are more likely to persist for multiple heating lines than for a single heating line when light ambient crossflows are introduced. Although simulation results should be viewed qualitatively, they suggest the potential importance of adjacent fire perimeters in actual wildland fire episodes for the development and behavior of buoyancy-generated horizontal roll vortices. FOR. SCI. 40(4):601–617.

ADDITIONAL KEY WORDS. Nonhydrostatic model, vorticity, pressure perturbations, circulation.

THE INTENSE HEAT ASSOCIATED WITH WILDLAND FIRES can generate very strong atmospheric boundary-layer circulations in the vicinity of the burning region. The production of hot gases within a wildland fire leads to buoyancy-generated upward velocities over the fire, and strong low-level horizontal flow into the burning area. Frequently, the boundary-layer circulations in the vicinity of a wildland fire will become organized to the extent that horizontal and columnar vortices are produced. There have been many observations and modeling efforts of columnar vortices or fire whirls in the vicinity of natural or manmade fires (Graham 1955, Dessens 1963, Byram and Martin 1970, Haines and Updike 1971, Church et al. 1980, Emori and Saito 1982, Church and Snow 1985, McRae and Flannigan 1990). Observations and modeling efforts of horizontal vortices have been less numerous. Haines (1982) presented documented evidence of horizontal roll vortices from nine sources. Haines and Smith (1983, 1987, 1992) and Smith et al. (1986, 1989) performed wind-tunnel experiments of horizontal roll vortex development over heated wires and ribbons. Two-dimensional modeling of horizontal roll vortices has been reported by Luti (1980, 1981), Heilman and Fast (1991, 1992), and Heilman (1992).

Church et al. (1980) provide a thorough discussion of the physical mechanisms

involved in the formation of horizontal roll vortices in the vicinity of a burning area. These mechanisms include reorientation and stretching of horizontal vorticity in the lower atmospheric boundary layer, concentration and amplification of vertical vorticity in the lower boundary layer, and generation of vorticity from buoyancy and surface drag forces. Haines (1982) hypothesized that horizontal roll vortices generated by buoyancy forces could play a role in the development of unburned tree-crown streets in crown-fire episodes if the downdraft portions of the vortices are sufficiently strong to inhibit the ignition of crowns by surface flames. If multiple burning regions are present in close proximity to each other during a wildland fire episode, the potential exists for a reinforcement of the downdraft portions of buoyancy-generated horizontal roll vortices that may be present between the burning regions. Downdraft reinforcement could, in turn, aid in the creation of unburned tree-crown streets in the areas between the burning regions.

Recent modeling and experimental evidence also suggests that the vortex circulations associated with *individual* lines of extreme surface heating are quite sensitive to ambient crossflow conditions (Heilman and Fast 1991, 1992, Heilman 1992, Haines and Smith 1992). This implies that small changes in speed and direction of the ambient boundary-layer flow could potentially alter the buoyancy-induced circulations over and near isolated surface and crown burning, and change the impact of horizontal roll vortices on unburned tree-crown street formation and the movement of flames, firebrands, and smoke. Unfortunately, the effect of ambient crossflow variations on vortex circulations over *multiple* lines of heating is not known.

In this study, we have attempted to test, through two-dimensional model simulations, the following hypotheses:

1. Multiple lines of extreme surface heating in close proximity to each other generate horizontal roll vortices that can interact and enhance downdraft speeds.
2. Multiple lines of extreme surface heating in close proximity to each other alter the impact of ambient crossflows on horizontal roll vortex development.
3. The structure of buoyancy-generated horizontal roll vortices in the vicinity of lines of extreme heating is very dependent on the spacing of the heating lines.

In this study, we have investigated the role of multiple heating lines in affecting vortex development by the mechanisms of buoyancy and surface drag forces alone. The mechanisms of reorientation and stretching of horizontal vorticity and the concentration and amplification of vertical vorticity are also involved in horizontal roll vortex development in actual wildland fire episodes (Church et al. 1980). These additional mechanisms are inherently three-dimensional in character and require a three-dimensional numerical model to capture their effects. However, horizontal roll vortex development by buoyancy and surface drag forces is a *two-dimensional* process. The two-dimensional character of this process makes it ideal for a two-dimensional modeling study and allows for a critical examination of multiple heating-line impacts on vortex development from buoyancy and surface drag forces alone, without the complicating factors of the other three-dimensional mechanisms.

MODEL OVERVIEW

Governing Equations

A two-dimensional nonhydrostatic atmospheric model was developed from the three-dimensional hydrostatic models of McCorcle (1988) and Fast and McCorcle

(1990) to investigate the boundary-layer conditions associated with extreme surface heating episodes. Prognostic equations are used to solve for the horizontal and vertical velocity components, the potential temperature, and the turbulent kinetic energy (TKE). The nonhydrostatic dynamic pressure perturbations are diagnosed from a Poisson equation derived from the atmospheric continuity equation. The two-dimensional governing equations are listed below (see the appendix for a list of symbols).

$$\frac{\partial U}{\partial t} = -U\frac{\partial U}{\partial x} - \omega\frac{\partial U}{\partial \xi}\frac{C}{\sigma} + \frac{\partial}{\partial \xi}\left(K_m\frac{\partial U}{\partial \xi}\frac{C}{\sigma}\right)\frac{C}{\sigma} + f(V - V_g) - \hat{f}\omega - \frac{1}{\rho}\frac{\partial p'}{\partial x} \quad (1)$$

$$\frac{\partial V}{\partial t} = -U\frac{\partial V}{\partial x} - \omega\frac{\partial V}{\partial \xi}\frac{C}{\sigma} + \frac{\partial}{\partial \xi}\left(K_m\frac{\partial V}{\partial \xi}\frac{C}{\sigma}\right)\frac{C}{\sigma} - f(U - U_g) \quad (2)$$

$$\frac{\partial \omega}{\partial t} = -U\frac{\partial \omega}{\partial x} - \omega\frac{\partial \omega}{\partial \xi}\frac{C}{\sigma} + \frac{\partial}{\partial \xi}\left(K_m\frac{\partial \omega}{\partial \xi}\frac{C}{\sigma}\right)\frac{C}{\sigma} - \frac{1}{\rho}\frac{\partial p'}{\partial \xi}\frac{C}{\sigma} - g\left(\frac{\rho'}{\rho}\right) \quad (3)$$

$$\frac{\partial \Theta}{\partial t} = -U\frac{\partial \Theta}{\partial x} - \omega\frac{\partial \Theta}{\partial \xi}\frac{C}{\sigma} + \frac{Q}{C_p}\left(\frac{p_o}{p}\right)^{R/C_p} + \frac{\partial}{\partial \xi}\left(K_h\frac{\partial \Theta}{\partial \xi}\frac{C}{\sigma}\right)\frac{C}{\sigma} \quad (4)$$

$$\frac{\partial e}{\partial t} = -U\frac{\partial e}{\partial x} - \omega\frac{\partial e}{\partial \xi}\frac{C}{\sigma} + \frac{\partial}{\partial \xi}\left(K_e\frac{\partial e}{\partial \xi}\frac{C}{\sigma}\right)\frac{C}{\sigma} + K_m\left[\left(\frac{\partial U}{\partial \xi}\right)^2 + \left(\frac{\partial V}{\partial \xi}\right)^2 + \left(\frac{\partial \omega}{\partial \xi}\right)^2\right]\left(\frac{C}{\sigma}\right)^2 - \frac{g}{T}K_h\frac{\partial \Theta}{\partial \xi}\frac{C}{\sigma} - \frac{K_m^3}{(c_1\ell)^4} \quad (5)$$

Equations (1)–(3) describe the time variation of the two horizontal velocity components (U and V) and the vertical velocity component (ω). Terms on the right side of Equation (1) are horizontal advection, vertical advection, turbulent diffusion, horizontal Coriolis force, horizontal pressure gradient force expressed in terms of the geostrophic wind component V_g, vertical Coriolis force, and the horizontal perturbation pressure gradient. Terms on the right side of Equation (2) are horizontal advection, vertical advection, turbulent diffusion, horizontal Coriolis force, and horizontal pressure gradient force expressed in terms of the geostrophic wind component U_g. The physical processes described on the right side of Equation (3) include horizontal advection, vertical advection, turbulent diffusion, acceleration due to the vertical perturbation pressure gradient, and buoyancy. Equation (4) describes the local time variation of the potential temperature and includes the processes of horizontal advection, vertical advection, heating due to infrared radiative flux, and turbulent diffusion. Because the turbulent diffusion processes modeled in Equations (1)–(4) are parameterized in terms of momentum and heat diffusivities that vary according to the local TKE of the atmosphere, a TKE prognostic equation is included in the model. The time variation in TKE is described in Equation (5) and includes the processes of horizontal advection, vertical advection, turbulent diffusion, mechanical production of turbulence due to shears in the wind field, buoyancy production or dissipation of TKE, and nonbuoyant dissipation of TKE. All the governing equations assume horizontal homogeneity along the horizontal y-axis. Only variations along the horizontal x-axis and the vertical ξ-axis are modeled by the two-dimensional equations. A complete description of the model and a discussion of the technique for determining the nonhydrostatic pressure perturbations can be found in Heilman and Fast (1992).

The governing equations are numerically solved by both finite-element and finite-difference techniques. A Galerkin finite-element expression (Paegle and McLawhorn 1983) is used to represent vertical diffusion, while finite differences are used to approximate advections, pressure gradients, and TKE production terms. The Crank-Nicholson method is utilized to integrate the prognostic equations forward in time.

The model domain spans a 2.0 km wide by 1.8 km high vertical plane. The governing equations are solved on a grid structure containing 656 grid points, with 41 grid points in the horizontal x-direction and 16 grid points in the vertical ξ-direction. A logarithmic vertical grid spacing is employed from the surface up to about 100 m. Above 100 m, the vertical grid spacing is uniform. This grid structure results in a minimum grid spacing of 0.17 m just above the surface and a maximum grid spacing of 188 m from a height of 100 m up to the model top at 1.8 km. A uniform grid spacing of 50 m is used in the horizontal.

Extreme surface heating like that associated with wildland fires can generate very strong local winds and large temperature gradients. In order to adequately resolve such atmospheric phenomena in numerical models, model grid spacings must be kept small. Small grid spacings, in turn, require small time-steps in the model simulations to ensure numerical stability over the range of atmospheric conditions being modeled (Anderson et al. 1984). Because of the fine grid structure used near the surface for the simulations in this study, a very small time-step (0.05 s) is required to preserve numerical stability. Simulations are carried out for a period of 90 s, resulting in 1800 time-steps per simulation.

For simplicity, the presence of multiple surface burning regions is approximated by introducing a constant surface temperature of 1500°K at three different locations in the modeled domain. Although this approximation does not adequately account for the large vertical temperature gradients that can occur between the surface and the region immediately above burning tree crowns, it is deemed sufficient for examining vortex behavior and development at elevations above typical tree crowns. A soil heat-flux equation (McCorcle 1988) is used to compute surface temperatures at each time step at all other surface locations. The relations of Paulson (1970), Businger et al. (1971), and Mellor and Yamada (1974) are used to describe the surface-layer values of the other atmospheric mean and turbulence-related variables. The vertical gradients of the dynamic pressure perturbations are set to zero at the surface.

At the model top, the horizontal wind field is assumed to be geostrophic and externally specified, while the vertical velocity component is set to zero there. The vertical gradients of potential temperature, TKE, and dynamic pressure perturbations are assumed to be zero at the model top. On the lateral boundaries, horizontal gradients for all variables except the dynamic pressure perturbations are set to zero. The pressure perturbations themselves are assumed to be zero along the lateral boundaries.

Initial logarithmic crossflow velocities (U) are assumed to be horizontally homogeneous and set by specifying initial friction velocities of 0.0 m s^{-1}, 0.05 m s^{-1}, 0.1 m s^{-1}, or 0.2 m s^{-1} for the different simulations. These friction velocities produce model-top crossflow speeds of 0.0 m s^{-1}, 1.43 m s^{-1}, 2.86 m s^{-1}, or 5.73 m s^{-1}, respectively. The initial velocity component in the y-direction (V)

is also assumed to be logarithmic and horizontally homogeneous, with a value of 5.73 m s^{-1} at the model top. An initial adiabatic atmosphere is assumed, with the potential temperature set at 298°K everywhere except at the defined "hot" surface grid points. At those locations, the surface potential temperature is set at 1500°K and held constant throughout each simulation. Initial soil temperatures of 298°K are also specified at all locations except at the "hot" surface grid points, where a temperature of 1500°K is set. Initial TKE values are diagnosed from level-2 of the Mellor and Yamada (1974) turbulence hierarchy.

NUMERICAL RESULTS

THREE LINES OF HEATING; 200 m SPACING

Because horizontal homogeneity in the y-direction is assumed for the two-dimensional simulations in this study, the "hot" surface grid points will be referred to as *heating lines*. The two-dimensional fields discussed in this section are actually vertical cross-sections of the atmosphere oriented perpendicular to the heating lines. Figures 1a–1d show the simulated two-dimensional velocity fields over a surface with heating lines located at x = 800 m, x = 1000 m, and x = 1200 m under varying crossflow windspeed conditions. The development of buoyancy-generated horizontal roll vortices is clearly evident when there is no ambient crossflow (Figure 1a). The vortices adjacent to the heating lines are centered at

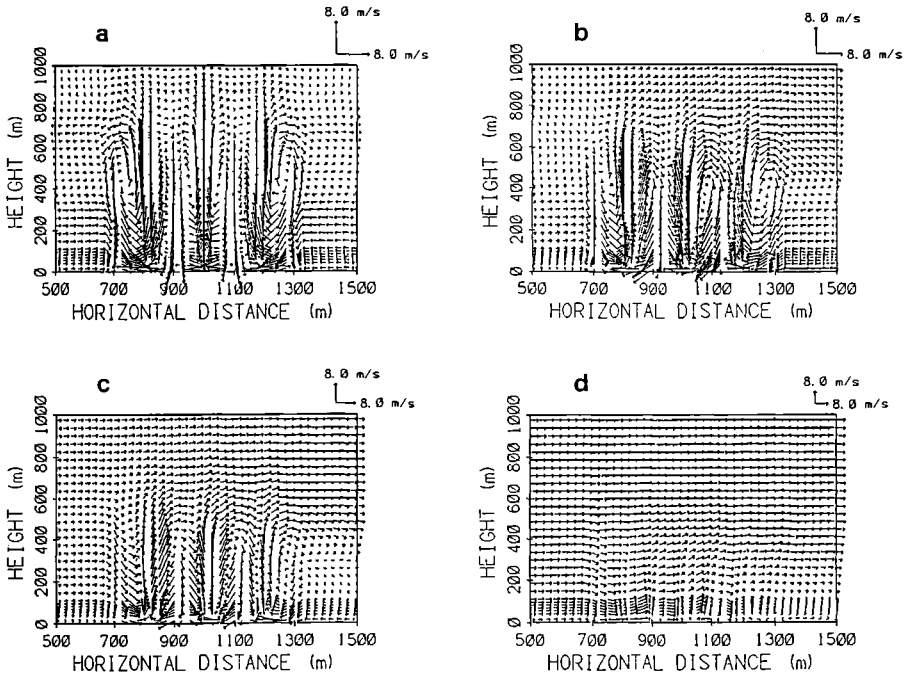

FIGURE 1. Simulated two-dimensional wind fields resulting from a surface temperature of 1500°K at x = 800 m, x = 1000 m, and x = 1200 m with (a) no ambient U-velocity, and light ambient U-velocities corresponding to initial friction velocities of (b) 0.05 m s^{-1}, (c) 0.1 m s^{-1}, and (d) 0.2 m s^{-1}. Velocity vectors indicate speed and direction at the base of the vectors.

roughly 400 m above the surface. The relatively close spacing of the heating lines allows for a substantial reinforcement of the downdrafts in regions between the heating lines. A comparison of the maximum downdraft speeds simulated in this study with those simulated in response to a single heating line (Heilman and Fast 1992) reveals an increase in the maximum downdraft speed of about 37%. In addition, the simulations indicate that significant downdrafts reach much closer to the surface when relatively closely spaced heating lines are present.

When no ambient crossflow is present, the simulated circulation about the central heating line is nearly symmetric. Strong low-level inflow induced by buoyancy effects appears on both sides of the central heating line, with negligible horizontal flow directly above the heating line. This is in contrast to the induced inflow appearing in the vicinity of the outer heating lines, where the winds have significant horizontal components directly over the heating lines. Only at heights above 100 m do the wind vectors become predominantly vertical.

Increasing the ambient crossflow wind speed distorts the circulation patterns in the vicinity of the three heating lines, with the characteristics of distortion dependent on the location of the individual heating lines in relation to the ambient crossflow direction (see Figures 1b and 1c). The presence of a light ambient crossflow ($\mu_* = 0.05$ m s^{-1} and $\mu_* = 0.1$ m s^{-1}) tends to inhibit the development of a buoyancy-generated horizontal roll vortex immediately upwind of the heating line at $x = 800$ m. Vortex development is also inhibited immediately upwind of the remaining heating lines, but the wind shears in these regions are much more significant than the shears upwind of the heating line at $x = 800$ m. Clockwise circulations with strong downdrafts persist on the leeward sides of all the heating lines. Unlike the simulation results for single heating lines (Heilman and Fast 1991, 1992), simulation results in this study suggest that buoyancy associated with multiple heating lines in close proximity to each other can lead to significant vortex activity above 100 m just downwind of the heating lines when a light ambient crossflow exists. Instead of destroying the vortices on the leeward sides of the heating lines, the ambient crossflow tends to lower the vertical extent of the vortices, with the vortex at 1200 m $< x <$ 1300 m showing the greatest drop in altitude. Between the heating lines, downdrafts remain strong down to the surface. Only after the initial friction velocity is increased to 0.2 m s^{-1} (model-top ambient wind speed of 5.73 m s^{-1}) does the vortex activity cease (see Figure 1d).

An interesting feature revealed in the multiple heating-line simulations is the strong horizontal component of the low-level wind vectors directly over the outside heating lines when no ambient crossflow is present. Figures 2a–2c show the vertical profiles of the horizontal velocity component directly over the three heating lines. Over the outside heating lines, there are inflow horizontal wind components of about 4.5 m s^{-1} below 50 m in the absence of an ambient crossflow (Figures 2a and 2c). Over the interior heating line, the wind vectors are nearly vertical (Figure 2b). This low-level inflow toward the interior heating line can be attributed to thermal-wind principles. The circulations in the region between the outside heating lines act to distribute heat over the whole interior region so that average temperatures in the interior region are higher than the temperatures encountered in the ambient air outside of the region bounded by the heating lines. This temperature gradient is the source of the simulated induced low-level horizontal inflow directly over the outside heating lines. The implication of this induced flow in an actual wildland fire with an ambient mean wind parallel to the flank

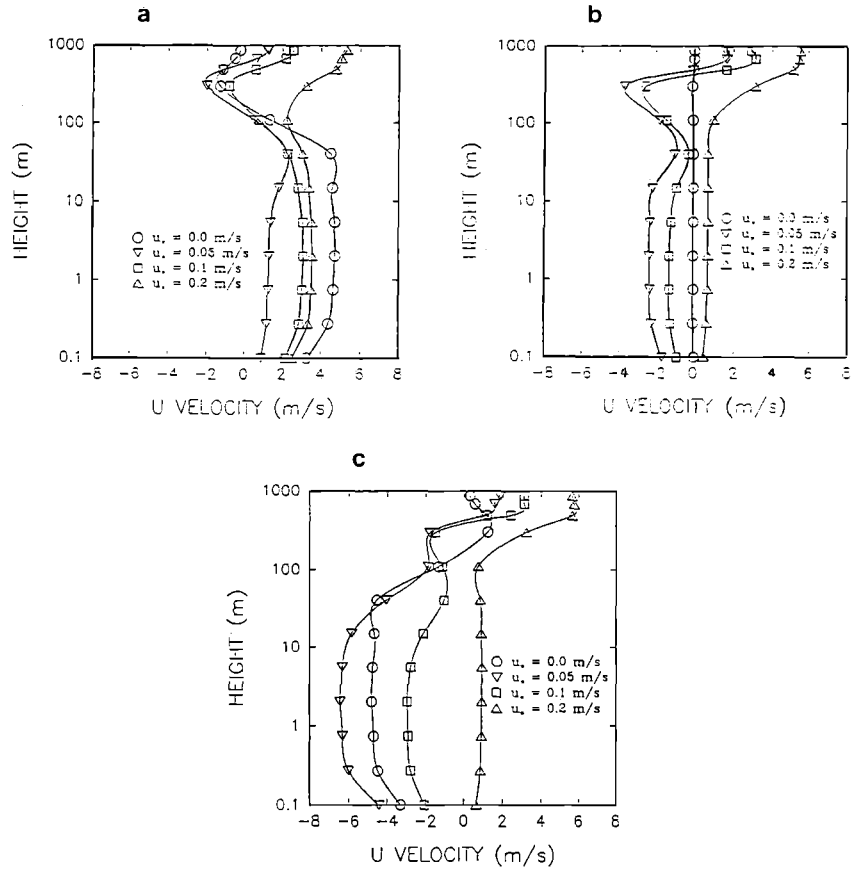

FIGURE 2. Ambient crossflow wind effects on the simulated U-velocity vertical profiles directly over the surface heating lines at (a) x = 800 m, (b) x = 1000 m, and (c) x = 1200 m.

of a burning area is the creation of nonparallel or curved burned regions in response to the wind-driven movement of surface or crown flames. There have been a number of observations of curved unburned tree-crown streets in the aftermath of wildland fire episodes (Haines 1982). If buoyancy-generated horizontal roll vortices develop in response to crown burning, then the potential exists for the downdraft segments of these vortices to inhibit crown burning in regions adjacent to fire flanks and to create sections of unburned crowns according to the orientation of the roll vortices.

As the initial friction velocity is increased from 0.0 m s^{-1} to 0.05 m s^{-1}, the simulations indicate an intensification of the low-level horizontal inflow components from the leeward sides of the heating lines. This intensification is the direct result of the lower portions of the clockwise vortices on the leeward sides of the heating lines becoming more vigorous. Figure 2a shows the horizontal U-velocity below 20 m decreasing from about 4.5 m s^{-1} to about 1.5 m s^{-1} over the windward heating line. When the initial friction velocity is increased to 0.1 m s^{-1} and 0.2 m s^{-1}, the low-level U-velocities increase, but they remain less than the velocities when no ambient crossflow is present. Figures 2b and 2c indicate the same general behavior over the central and leeward heating lines, respectively.

The two-dimensional vorticity fields ($\zeta = \partial\omega/\partial x - \partial U/\partial \xi$) corresponding to the wind fields in Figures 1a–1d are shown in Figures 3a–3d. Vorticity is a measure of the rotation of the wind field, with positive and negative vorticity corresponding to counterclockwise and clockwise rotation, respectively. With no ambient cross-flow, the vorticity pattern is symmetric about the central heating line (Figure 3a). Maximum horizontal vorticity gradients appear over the central heating line at elevations between 200 m and 500 m. The upper-level vorticity maxima associated with the central heating line tend to exist at higher elevations than the vorticity maxima associated with the outer lines of heating. When the initial friction velocity is increased from 0.0 m s^{-1} to 0.05 m s^{-1}, the positive and negative vorticity maxima between the heating lines at x = 800 m and x = 1000 m are enhanced (Figure 3b). This indicates that the circulation between the heating lines at those locations has become more vigorous and is clearly observed in Figure 1b. An initial friction velocity of 0.1 m s^{-1} leads to a general reduction in the vorticity over the heating lines, with the vorticity just upwind of the heating

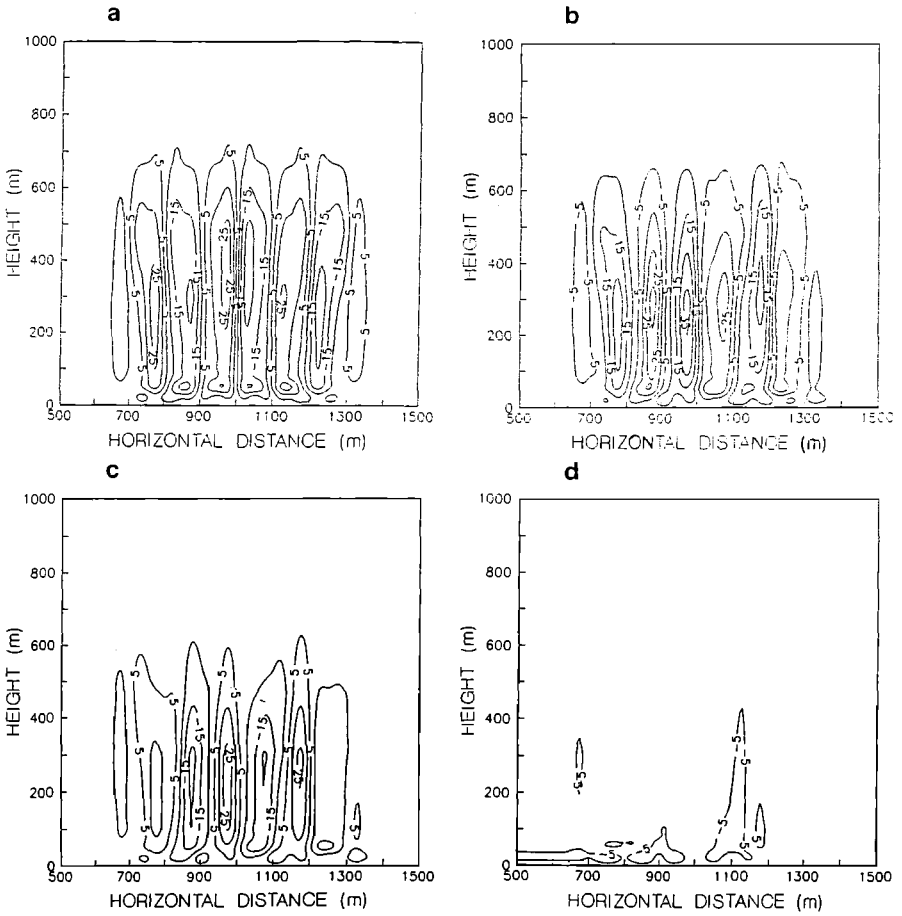

FIGURE 3. Simulated two-dimensional vorticity (x 100) fields resulting from a surface temperature of 1500°K at x = 800 m, x = 1000 m, and x = 1200 m with (a) no ambient U-velocity, and light ambient U-velocities corresponding to initial friction velocities of (b) 0.05 m s^{-1}, (c) 0.1 m s^{-1}, and (d) 0.2 m s^{-1}.

line at $x = 800$ m showing the largest decrease (Figure 3c). At this location, the wind field develops a wave, but no closed circulation. The vorticity magnitudes are greatly reduced when the initial friction velocity is increased to 0.2 m s^{-1} (Figure 3d).

The present simulations suggest the importance of the interaction of individual buoyancy-generated horizontal roll vortices, as described by Church et al. (1980). When the sources of heating are sufficiently close to each other, vortices can enhance the downdrafts between the heating sources. One of the mechanisms which has been hypothesized for contributing to the development of unburned tree-crown streets is the horizontal roll vortex (Haines 1982). Conceptual models suggest that downdrafts from individual roll vortices can inhibit the burning of tree crowns. Haines and Smith (1987) presented evidence that downdrafts in the vicinity of wildland fires can be quite intense and of sufficient strength to inhibit the movement of flames upward into the tree-crown region. If horizontal roll vortices are indeed involved in the formation of unburned tree-crown streets during wildland fire episodes, then adjacent horizontal roll vortices would tend to enhance downdraft wind speeds and further inhibit the burning of crowns just beyond the flanks of the burning regions. Only relatively low intensity understory burning would tend to prevail in the region where strong downdrafts are present. The present simulations do not describe the mechanisms involved in the formation of new heating sources, but rather assume the *existence* of multiple heating lines (i.e., burning regions). Observational evidence presented by Haines and Smith (1987) suggests that the initiation of secondary fires adjacent to an existing burning area can be accomplished by the deposition of firebrands beyond the flanks of the existing burning area by low-level vortex activity, thereby creating additional heating lines that generate new vortex pairs. The initial distance between adjacent fires, in this case, is dependent on the extent of the movement of firebrands beyond the flanks of the burning regions. Typical separation distances between adjacent unburned tree-crown streets have been observed to be on the order of 50 m to 800 m (Haines 1982), indicating similar separation distances between adjacent burning areas. Regardless of the mechanisms involved in the formation of multiple heating lines, the present simulations reveal that once multiple heating lines have been established in close proximity to each other, powerful downdrafts between the heating lines can be generated.

The present simulations also suggest that buoyancy-generated horizontal roll vortices associated with multiple heating lines are more likely to persist than vortices associated with a single heating line when light ambient crossflows develop. Results from single heating-line simulations reveal that light ambient crossflows are more likely to destroy upper-level vortices (Heilman and Fast 1991, 1992). On the other hand, vortices associated with downwind heating lines tend to remain intact, especially on the downwind sides of the individual heating lines. Figures 1b and 1c indicate that the upwind heating line acts as a "barrier" for the remaining heating lines and allows rather vigorous vortex activity to persist in the presence of an ambient crossflow of sufficient strength to inhibit the development of vortices around a single heating source.

The low-level, dynamic nonhydrostatic pressure perturbations that develop in response to the convergent and divergent characteristics of the circulation fields of Figures 1a–1d are shown in Figure 4. Positive and negative pressure perturbations correspond to wind-field convergence and divergence, respectively. With

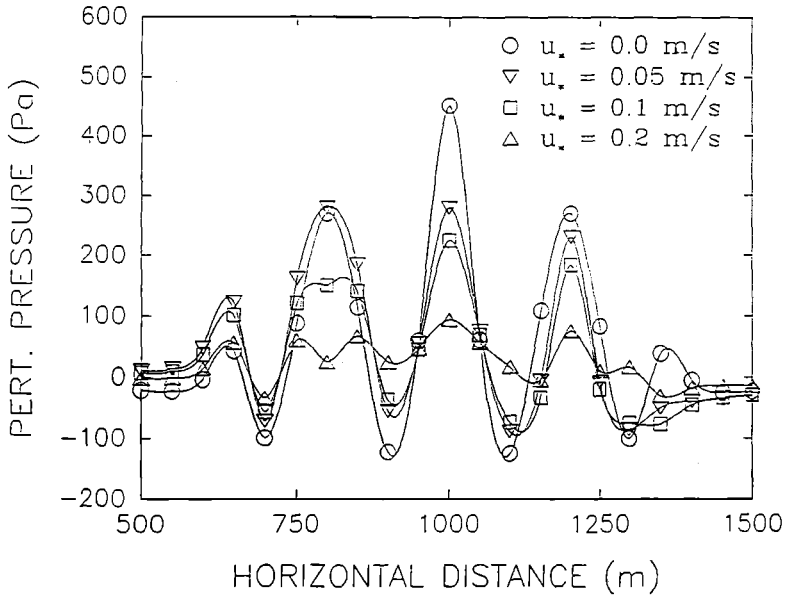

FIGURE 4. Ambient crossflow wind effects on the simulated nonhydrostatic pressure perturbations at a height of 110 m with a surface temperature of 1500°K at x = 800 m, x = 1000 m, and x = 1200 m.

no ambient crossflow, the maximum pressure perturbation is simulated over the central heating line. Maximum perturbation pressures are about 40% smaller over the outside heating lines. The difference in maximum perturbation values is due to the wind-field convergence characteristics over the modeled domain. Over the central heating line, the symmetric low-level horizontal inflow produces a region of maximum convergence that results in a region of high nonhydrostatic dynamic pressure. Over the outer heating lines, convergence also characterizes the wind field, but it is weaker due to the asymmetric pattern of the low-level circulation. The weaker convergence leads to smaller perturbation pressure maxima over the outer heating lines. When the ambient crossflow wind speed increases, the maximum perturbation pressure over the central heating line shows a marked decrease and has a value similar to the maximum pressures over the outer heating lines. The interaction of the ambient crossflow with the buoyancy-induced circulations reduces the wind-field convergence values as the ambient crossflow wind speed increases. Figure 4 also shows the distinct reduction in perturbation pressure values as the initial friction velocity is increased to 0.2 m s^{-1}.

THREE LINES OF HEATING; 300 m SPACING

Figures 5a–5d show the simulated wind fields for different ambient crossflow conditions when the heating lines are placed at x = 700 m, x = 1000 m, and x = 1300 m. The most obvious difference between the wind fields for the 200 m and 300 m heating-line spacings for the no-ambient-crossflow cases is the reduction in downdraft speeds in the region between the heating lines when the spacing is increased to 300 m. Because the individual roll vortices associated with each heating line have a simulated width of about 100 m, the reinforcement of down-

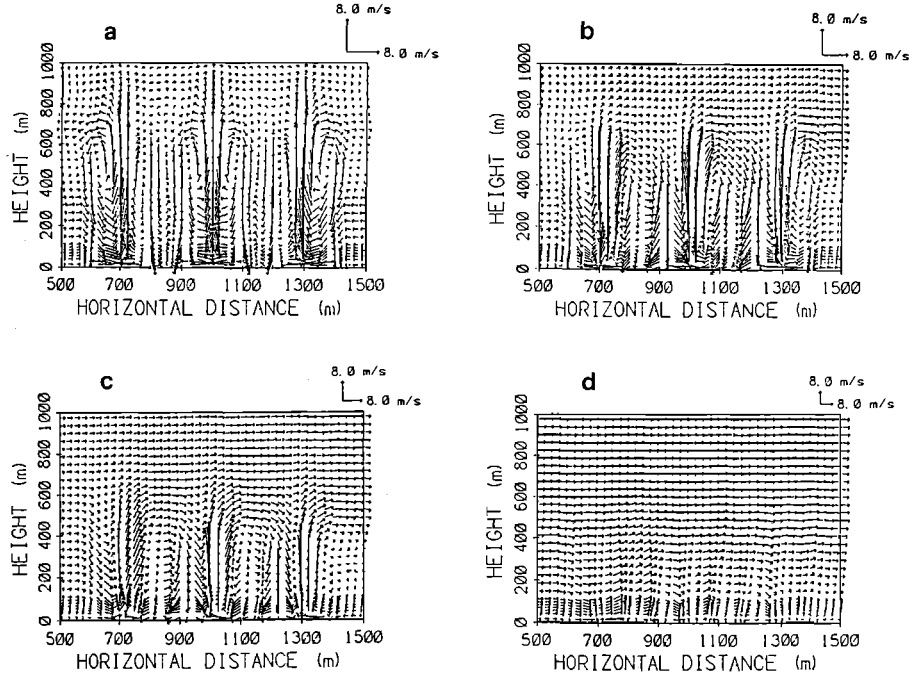

FIGURE 5. Simulated two-dimensional wind fields resulting from a surface temperature of 1500°K at x = 700 m, x = 1000 m, and x = 1300 m with (a) no ambient U-velocity, and light ambient U-velocities corresponding to initial friction velocities of (b) 0.05 m s^{-1}, (c) 0.1 m s^{-1}, and (d) 0.2 m s^{-1}. Velocity vectors indicate speed and direction at the base of the vectors.

drafts by adjacent roll vortices is reduced by increasing the heating-line spacing to 300 m. The circulations over each heating line tend to approach the circulation over single heating lines, as depicted in Heilman and Fast (1992). With no ambient crossflow, the circulation about the central heating line remains symmetric. Directly over the outside heating lines, the low-level wind vectors still have horizontal components, but they are significantly smaller than for the 200 m spaced heating lines. With the heating lines farther apart, the horizontal temperature gradient between the ambient air outside the region bounded by the heating lines and the air inside the region is less. This leads to a reduction in the induced horizontal flow from thermal-wind principles.

The horizontal roll-vortex behavior undergoes marked changes with the introduction of an ambient crossflow. Each roll vortex immediately upwind of each heating line is destroyed when the initial friction velocity is set at 0.05 m s^{-1}, 0.1 m s^{-1}, or 0.2 m s^{-1}. The roll vortices on the leeward sides of the heating lines at x = 700 m and x = 1000 m persist until the initial friction velocity is increased to 0.2 m s^{-1}, but they decrease in elevation as the ambient crossflow increases. On the leeward side of the heating line at x = 1300 m, the roll vortex is less vigorous than when the heating lines are 200 m apart for an initial ambient friction velocity of 0.1 m s^{-1} (see Figures 1c and 5c). Vortex behavior is essentially destroyed when the initial friction velocity is increased to 0.2 m s^{-1}, although the presence of multiple heating lines allows low-level convergence and divergence to be more prominent than with single lines of heating (Heilman and Fast 1992).

With the heating lines spaced 300 m apart, the lower portion of the horizontal

roll vortices on the leeward sides of the heating lines do not intensify to the degree that was noted for the 200 m spaced heating lines when the initial ambient friction velocity is increased from 0.0 m s^{-1} to 0.05 m s^{-1}. This results in less variation in the low-level vertical profiles of U-velocity over the heating lines, as shown in Figures 6a–6c. The low-level U-velocities over the windward and central heating lines decrease slightly as the initial friction velocity is increased to 0.05 m s^{-1}. Over the leeward heating line, the low-level U-velocity remains about the same below 10 m and increases between 10 m and 100 m. A further increase in the ambient crossflow results in low-level U-velocities becoming more positive. Low-level negative U-velocities over the central and leeward heating lines are essentially absent after the initial ambient friction velocity is increased to 0.1 m s^{-1}. This is in contrast to the 200 m spaced heating-line simulations, where low-level U-velocities remained negative over the central and leeward heating lines for the same ambient crossflow.

With heating lines spaced 300 m apart, the magnitudes of the positive and negative vorticity maxima (not shown) for the no-ambient-crossflow conditions are similar to the vorticity magnitudes simulated over the heating lines spaced 200 m apart. However, there is a tendency for the vorticity maxima generated by the

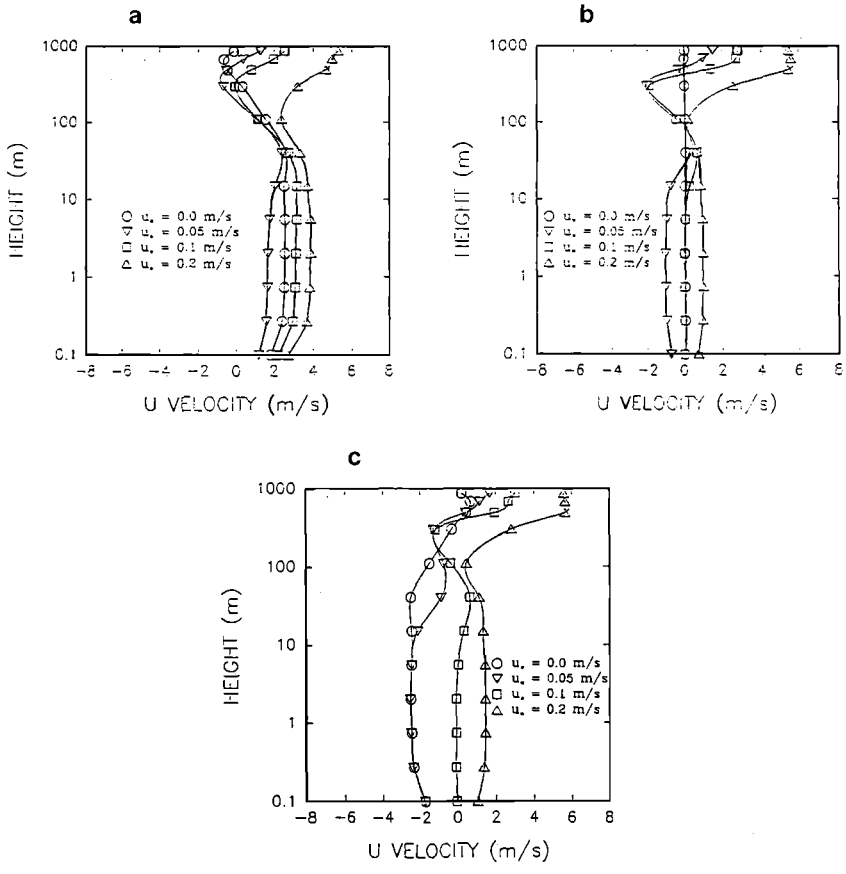

FIGURE 6. Ambient crossflow wind effects on the simulated U-velocity vertical profiles directly over the surface heating lines at (a) x = 700 m, (b) x = 1000 m, and (c) x = 1300 m.

outside heating lines to move to higher elevations when the heating lines are spaced farther apart. As the spacing is increased, the vorticity patterns associated with the outside heating lines begin to resemble the vorticity pattern of the central heating line, which is also quite similar to the pattern over a single heating line (Heilman and Fast 1992). Increasing the spacing of the heating lines also has a major impact on vorticity fields when an ambient crossflow is present. The vorticity values are significantly reduced over and adjacent to the upwind heating line when the heating lines are placed farther apart. The vorticity values in the vicinity of the central heating line are diminished as well, but not nearly to the extent as over the upwind heating line. The vorticity in the vicinity of the downwind heating line is least affected by increasing the spacing of the heating lines.

With no ambient crossflow, the larger distance between heating lines results in larger peak nonhydrostatic pressure perturbation values (not shown) over the heating lines than for the heating lines spaced 200 m apart. The heating lines spaced 300 m apart act more like isolated heating lines that generate symmetric circulation patterns, with significant low-level flow convergence directly over the surface heating lines and larger pressure perturbations. Increasing the heating-line spacing also results in the generation of secondary pressure perturbation maxima between the heating lines. These maxima represent regions of flow convergence in the downdraft portions of the circulations generated by surface heating.

Three Lines of Heating; 100 m Spacing

A third set of simulations was performed to determine the behavior of buoyancy-induced horizontal roll vortices when the heating-line spacing is reduced to the characteristic width of the vortices. Figures 7a–7d show the degree of horizontal roll vortex development in response to different ambient crossflow conditions when the heating lines are placed at $x = 900$ m, $x = 1000$ m, and $x = 1100$ m. The small spacing between heating lines inhibits the development of any downdrafts between them. A broad region of relatively strong updrafts exists at 900 m $< x <$ 1100 m with no ambient crossflow (Figure 7a). Horizontal roll vortices only develop outside the region bounded by the heating lines. The introduction of a light ambient crossflow destroys the upwind roll vortex and produces a less vigorous upper-level downwind vortex at about $x = 1200$ m (Figure 7b). Further increases in the ambient crossflow speed destroy this upper-level vortex while generating a low-level vortex centered at $x = 1175$ m at a height of about 100 m (Figure 7c). These simulations indicate that if the heating lines are sufficiently close together, they produce circulation patterns that resemble the patterns associated with a single heating line. The buoyancy forces generated by each heating line produce updrafts over and between the heating lines that overcome any tendency for induced downward motion. In effect, the boundary-layer circulation responds to the multiple heating lines as if they were equivalent to one broad continuous area of surface heating. The nonhydrostatic dynamic pressure perturbations that develop over the closely spaced heating lines (not shown) show a region of positive perturbations between the outer heating lines, which is in contrast to the periodic negative perturbations that develop over the heating lines spaced 200 m and 300 m apart. The behavior of the pressure perturbations is the

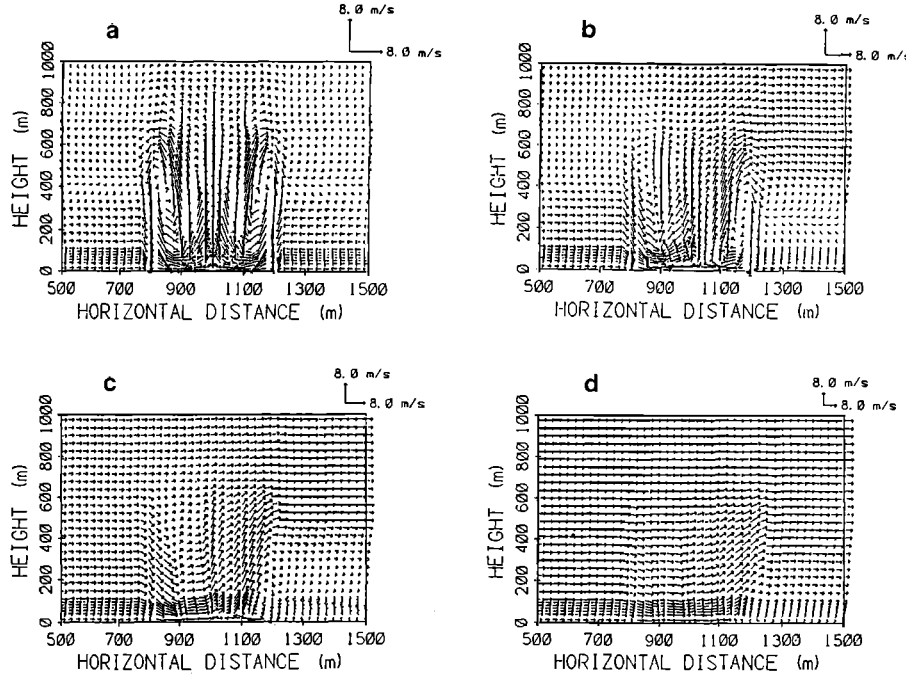

FIGURE 7. Simulated two-dimensional wind fields resulting from a surface temperature of 1500°K at x = 900 m, x = 1000 , and x = 1100 m with (a) no ambient U-velocity, and light ambient U-velocities corresponding to initial friction velocities of (b) 0.05 m s^{-1}, (c) 0.1 m s^{-1}, and (d) 0.2 m s^{-1}. Velocity vectors indicate speed and direction at the base of the vectors.

direct result of inhibited downdraft activity between the heating lines spaced 100 m apart.

SUMMARY AND CONCLUSIONS

Simulated two-dimensional roll vortices that develop in response to the buoyancy mechanism, as outlined by Church et al. (1980), are quite sensitive to the existence of multiple heating lines as well as ambient crossflow wind speeds. Depending on the spacing of the individual heating lines, horizontal roll vortex development and behavior undergoes marked changes when ambient crossflow conditions are varied. During calm crossflow periods, buoyancy-induced horizontal roll vortex pairs develop over the individual heating lines if they are sufficiently far apart. The numerical simulations suggest a minimum spacing for vortex development of this type to be on the order of the horizontal dimension of the vortices. A critical heating-line spacing for vortex interaction and downdraft reinforcement between heating lines is also suggested from the simulations. With the heating-line spacing set at 200 m, downdraft wind speeds increase by about 37% over the speeds previously simulated with only one heating line. Downdraft reinforcement by adjacent horizontal roll vortices in actual wildland fire episodes could inhibit the burning of tree crowns and aid in the development of unburned tree-crown streets between discrete burning regions.

Low-level horizontal flow directly over the outside heating lines and directed toward the central heating line is observed in the simulations when no ambient crossflow is present. The thermal characteristics of the boundary layer inside and outside the region bounded by the heating lines lead to significant horizontal wind components directly over the outside heating lines and is more pronounced when the heating lines are moved closer together. In an actual wildland fire with adjacent but discrete burning areas and an ambient flow parallel to the flanks of the burning areas, this phenomenon suggests a migration of flames toward the interior burning area. The generation of curved unburned tree-crown streets in response to the downdraft segments of the accompanying migrating roll vortices is also suggested.

The presence of multiple heating lines also affects the development and behavior of horizontal roll vortices generated by the buoyancy mechanism when light ambient crossflows are present. Upwind heating lines in the presence of a light ambient crossflow tend to act as "barriers" to the flow for the downwind heating line. Simulations indicate that horizontal roll vortex activity on the leeward sides of the downwind heating lines is more pronounced than for a single heating line. An increase in vortex activity adjacent to a downwind fire flank during an actual wildland fire episode with varying ambient crossflow conditions could pose a potential threat to firefighter safety in that region.

The simulation results from this study should be viewed qualitatively. Observations of horizontal roll vortices in actual wildland fire episodes have been limited to photographs and measurements of unburned tree-crown streets that support horizontal roll vortex occurrence. The lack of observational data makes model verification very difficult. Comparisons of the two-dimensional model results with the wind-tunnel experiments of Haines and Smith (1983, 1992) for a single heating line show good qualitative agreement under calm and light ambient crossflow conditions. Experiments indicate a decrease in elevation of horizontal roll vortices immediately downwind of a single heating line when a light ambient crossflow is introduced. Model simulations from this study indicate a similar behavior for vortices immediately downwind of the most leeward heating line when multiple heating lines are present. Although the model simulations and experimental results compare favorably, comparisons of this nature must be done carefully in light of the scale discrepancies between atmospheric boundary-layer processes and the wind-tunnel structures observed by Haines and Smith (1983, 1992). Flow structures inside small wind tunnels are generally characterized by length scales that are much closer to the dissipative end of the turbulence spectrum than phenomena occurring in the atmospheric boundary layer.

Horizontal roll vortex development during a wildland fire is an inherently three-dimensional process involving the interactions of the ambient boundary-layer flow and the induced flow from buoyancy effects. The two-dimensional simulations performed in this study attempt to capture the two-dimensional circulations that develop from buoyancy effects alone. Three-dimensional simulations are required to address all the mechanisms involved in horizontal roll vortex development, as described by Church et al. (1980). Nevertheless, the two-dimensional simulations performed in this study reveal the sensitivity of buoyancy-generated horizontal roll vortices to multiple heating-line spacings and ambient crossflow wind speeds.

LITERATURE CITED

ANDERSON, D.A., J.C. TANNEHILL, and R.H. PLETCHER. 1984. Computational fluid mechanics and heat transfer. McGraw-Hill, New York, 599 p.

BUSINGER, J.A., J.C. WYNGAARD, Y. IZUMI, and E.F. BRADLEY. 1971. Flux-profile relationships in the atmospheric surface layer. J. Atmos. Sci. 28:181–189.

BYRAM, G.M., and R.E. MARTIN. 1970. The modeling of fire whirlwinds. For. Sci. 16:386–399.

CHURCH, C.R., and J.T. SNOW. 1985. Observation of vortices produced by the Météotron. J. Rech. Atmos. 19:455–467.

CHURCH, C.R., J.T. SNOW, and J. DESSENS. 1980. Intense atmospheric vortices associated with a 1000 MW fire. Bull. Am. Meteor. Soc. 61:682–694.

DESSENS, J. 1963. Tourbillon de sable prés de l'incendie du puits de Gassi-Touil. J. Rec. Atmos. 1:290.

EMORI, R.I., and K. SAITO. 1982. Model experiment of a hazardous forest fire whirl. Fire Tech. 18:319–327.

FAST, J.D., and M.D. MCCORCLE. 1990. A two-dimensional numerical sensitivity study of the Great Plains low-level jet. Mon. Wea. Rev. 118:151–163.

GRAHAM, H.E. 1955. Fire whirlwinds. Bull. Am. Meteor. Soc. 36:99–103.

HAINES, D.A. 1982. Horizontal roll vortices and crown fires. J. Appl. Meteor. 21:751–763.

HAINES, D.A., and M.C. SMITH. 1983. Wind tunnel generation of horizontal roll vortices over a differentially heated surface. Nature 306:351–352.

HAINES, D.A., and M.C. SMITH. 1987. Three types of horizontal vortices observed in wildland mass and crown fires. J. Clim. Appl. Meteor. 26:1624–1637.

HAINES, D.A., and M.C. SMITH. 1992. Simulation of the collapse of bent-over vortex pairs observed in wildland fires. For. Sci. 38:68–79.

HAINES, D.H., and G.H. UPDIKE. 1971. Fire whirlwind formation over flat terrain. USDA For. Serv. Res. Pap. NC-71. 12 p.

HEILMAN, W.E. 1992. Atmospheric simulations of extreme surface heating episodes on simple hills. Int. J. Wild. Fire 2:99–114.

HEILMAN, W.E., and J.D. FAST. 1991. Two-dimensional numerical simulations of atmospheric conditions near lines of extreme surface heating. P. 541–548 *in* Proc. 11th Conf. Fire & For. Meteor. Society of American Foresters, Bethesda, MD.

HEILMAN, W.E., and J.D. FAST. 1992. Simulations of horizontal roll vortex development above lines of extreme surface heating. Int. J. Wildland Fire 2:55–68.

LUTI, F.M. 1980. Transient flow development due to a strong heat source in the atmosphere. Part I: Uniform temperature source. Combust. Sci. Tech. 23:163–175.

LUTI, F.M. 1981. Some characteristics of a two-dimensional starting mass fire with cross flow. Combust. Sci. Tech. 24:25–33.

MCCORCLE, M.D. 1988. Simulation of surface-moisture effects on the Great Plains low-level jet. Mon. Wea. Rev. 116:1705–1720.

MCRAE, D.J., and M.D. FLANNIGAN. 1990. Development of large vortices on prescribed fires. Can. J. For. Res. 20:1878–1887.

MELLOR, G.L., and T. YAMADA. 1974. A hierarchy of turbulence closure models for planetary boundary layers. J. Atmos. Sci. 31:1791–1806.

PAEGLE, J., and D.W. MCLAWHORN. 1983. Numerical modeling of diurnal convergence oscillations above sloping terrain. Mon. Wea. Rev. 111:67–85.

PAULSON, C.A. 1970. The mathematical representation of wind speed and temperature profiles in the unstable atmospheric surface layer. J. Appl. Meteor. 9:857–861.

SMITH, M.C., D.A. HAINES, and W.A. MAIN. 1986. Some characteristics of longitudinal vortices produced by line-source heating in a low-speed wind tunnel. Int. J. Heat Mass Transf. 29:59–68.

SMITH, M.C., D.A. HAINES, and W.A. MAIN. 1989. Growth of buoyancy-induced longitudinal vortex pairs in a laminar flow. Int. J. Heat Mass Transf. 323:1879–1885.

APPENDIX

List of Symbols

C	Constant in the vertical coordinate ξ definition
C_p	Specific heat at constant pressure
c_1	Constant in the dissipation term of the TKE equation
e	Turbulent kinetic energy
$f,\hat{f}$	Coriolis parameters
g	Gravitational acceleration
K_e	Diffusion coefficient for TKE
K_h	Heat diffusivity
K_m	Momentum diffusivity
ℓ	Vertical mixing length
$p_\circ$	Reference surface pressure (10^5 Pa)
p'	Nonhydrostatic pressure perturbation
Q	Heating due to infrared radiative flux
R	Gas constant for dry air
s	Height of model top
t	Time
U	Nonturbulent velocity component in x-direction
U_g	Thermally-induced pressure gradient in y-direction, expressed as a geostrophic velocity
u_*	Friction velocity
V	Nonturbulent velocity component in y-direction
V_g	Thermally induced pressure gradient in x-direction, expressed as a geostrophic velocity
x,z	Orthogonal Cartesian coordinates
z_g	Terrain height
θ	Potential temperature
$\xi = C \ln(\sigma/0.1)$	Transformed vertical coordinate in logarithmically spaced portion of model grid
ρ	Total atmospheric density
ρ'	Dynamic density perturbation
$\sigma = s(z - z_g)/(s - z_g)$	Vertical coordinate in the nonorthogonal coordinate system
ω	Nonturbulent velocity component in ξ-direction

Manuscript received June 7, 1993.

Author and Acknowledgments

W.E. Heilman is Research Meteorologist with the North Central Forest Experiment Station, USDA, Forest Service, 1407 S. Harrison Road, East Lansing, MI 48823.